







Article

Synthesis of Dense MgB₂ Superconductor via In Situ and Ex Situ Spark Plasma Sintering Method

Joseph Longji Dadiel^{1,*}, Sugali Pavan Kumar Naik^{2,3} , Paweł Pęczkowski⁴ , Jun Sugiyama¹, Hiraku Ogino^{1,3} , Naomichi Sakai^{1,*} , Yokoyama Kazuya⁵, Tymon Warski^{6,7} , Anna Wojcik⁸, Tetsuo Oka¹  and Masato Murakami¹

- ¹ Superconducting Materials Laboratory, Graduate School of Science and Engineering, Shibaura Institute of Technology, 3-7-5 Toyosu, Koto-Ku, Tokyo 135-8548, Japan; mb18017@shibaura-it.ac.jp (J.S.); h-ogino@aist.go.jp (H.O.); okat@sic.shibaura-it.ac.jp (T.O.); masatomu@shibaura-it.ac.jp (M.M.)
 - ² Department of Physics, Tokyo University of Science, 1 Chome-3 Kagurazaka, Shinjuku City, Tokyo 162-8601, Japan; spavankumarnaik@yahoo.in
 - ³ Research Institute for Advanced Electronics and Photonics, National Institute of Advanced Industrial Science and Technology (AIST), 1-1-1 Central 2, Umezono, Tsukuba 305-8568, Japan
 - ⁴ Institute of Physical Sciences, Faculty of Mathematics and Natural Sciences, School of Exact Sciences, Cardinal Stefan Wyszyński University, K. Wóycickiego 1/3 Street, 01-938 Warsaw, Poland; p.peczkowski@wp.pl or p.peczkowski@uksw.edu.pl
 - ⁵ Department of Electrical and Electronics, Faculty of Engineering, Ashikaga University, 286-1 Omae-cho, Ashikaga-Shi, Tochigi 326-8558, Japan; k-yokoyama@ashitech.ac.jp
 - ⁶ Łukasiewicz Research Network, Institute of Non-Ferrous Metals, Sowinskiego 5 Street, 44-100 Gliwice, Poland; tymon.warski@imn.gliwice.pl
 - ⁷ Department of Engineering Materials and Biomaterials, Faculty of Mechanical Engineering, Silesian University of Technology, Konarskiego 2a Street, 44-100 Gliwice, Poland
 - ⁸ Institute of Metallurgy and Materials Science, Polish Academy of Science, Reymonta 25 Street, 30-059 Krakow, Poland; a.wojcik@imim.pl
- * Correspondence: na19102@shibaura-it.ac.jp or dadielson@gmail.com; (J.L.D.); nsakai@shibaura-it.ac.jp (N.S.); Tel.: +81-(0)7-042-876-884 (J.L.D. & N.S.)



Citation: Dadiel, J.L.; Naik, S.P.K.; Pęczkowski, P.; Sugiyama, J.; Ogino, H.; Sakai, N.; Kazuya, Y.; Warski, T.; Wojcik, A.; Oka, T.; et al. Synthesis of Dense MgB₂ Superconductor via In Situ and Ex Situ Spark Plasma Sintering Method. *Materials* **2021**, *14*, 7395. <https://doi.org/10.3390/ma14237395>

Academic Editor: Israel Felner

Received: 9 November 2021

Accepted: 26 November 2021

Published: 2 December 2021

Publisher's Note: MDPI stays neutral with regard to jurisdictional claims in published maps and institutional affiliations.



Copyright: © 2021 by the authors. Licensee MDPI, Basel, Switzerland. This article is an open access article distributed under the terms and conditions of the Creative Commons Attribution (CC BY) license (<https://creativecommons.org/licenses/by/4.0/>).

Abstract: In this study, high-density magnesium diboride (MgB₂) bulk superconductors were synthesized by spark plasma sintering (SPS) under pressure to improve the field dependence of the critical current density (J_c - B) in MgB₂ bulk superconductors. We investigated the relationship between sintering conditions (temperature and time) and J_c - B using two methods, ex situ (sintering MgB₂ synthesized powder) and in situ (reaction sintering of Mg and B powder), respectively. As a result, we found that higher density with suppressed particle growth and suppression of the formation of coarse particles of MgB₄ and MgO were found to be effective in improving the J_c - B characteristics. In the ex situ method, the degradation of MgB₂ due to pyrolysis was more severe at temperatures higher than 850 °C. The sample that underwent SPS treatment for a short time at 850 °C showed higher density and less impurity phase in the bulk, which improved the J_c - B properties. In addition, the in situ method showed very minimal impurity with a corresponding improvement in density and J_c - B characteristics for the sample optimized at 750 °C. Microstructural characterization and flux pinning (f_p) analysis revealed the possibility of refined MgO inclusions and MgB₄ phase as new pinning centers, which greatly contributed to the J_c - B properties. The contributions of the sintering conditions on f_p for both synthesis methods were analyzed.

Keywords: MgB₂; spark plasma sintering; microstructure; flux pinning; critical current density; grain connectivity

1. Introduction

Since 1953, intermetallic MgB₂ with a hexagonal structure has been known [1]. Its superconducting critical temperature (T_c), up to 39 K, was observed in 2001 due to the presence of two distinct superconducting gaps [2]. The inexpensive cost, strong mechanical

properties [3,4], and long coherence length of this material make it ideal for a variety of applications [5]. It has a greater upper critical field than standard NbTi and Nb₃Sn superconductors. It has fewer anisotropic effects and no weak links as compared to superconducting cuprates. The grain boundaries do not act as weak links that inhibit superconducting current; therefore, this makes it possible to fabricate superconducting bulk and wires in crystalline forms [5,6].

The MgB₂ compound has been found to be one of the reliably promising materials for the next generation of superconductors due to its cost and relative density of 2.63 g/cm³, as well as its ease of manufacture due to its suitability for light-weight applications [1]. In the literature [6,7], we can find reports of research on this topic: the effects of the SPS temperature on the mechanical properties of the MgB₂ bulk superconductor were investigated through bending tests of specimens cut from the bulk samples. Both the Young modulus and bending strength were improved by an increase in the SPS temperature [8]. For better practical application, together with the superconducting properties of MgB₂, the critical current density (J_c) is important as it improves their mechanical properties [9]. However, since MgB₂ is polycrystalline in nature, most techniques for producing this material involve low relative densities that have poor material performance [10]. There is a solid relationship between the super-current conduction region and the material density, the resulting effect of which is constantly reflected in J_c [11,12]. Three different advances are used for the production of MgB₂ wires and bulk samples, hence: the ex situ technique [9,13,14], in situ [9,14–17], and the Mg Internal Diffusion (IMD) technique [18]. Gajda et al. [8,9] studied the fabrication of MgB₂ wire by hot isostatic pressure (HIP) and the influence of various physicochemical parameters on their superconducting properties. By applying SPS to fabricate sintered polycrystalline MgB₂ bulks in our research, the bulk superconducting performance has been studied in relation to our starting powders and techniques. The approach to target the J_c of the samples, by enhancing it as a result of the controlled microstructure and improved density and flux pinning, was achieved by optimizing the sintering temperature conditions for both in situ and ex situ SPS processing with reduced deterioration of the MgB₂ phase. The SPS process can be used to obtain full density without grain growth at a high heating rate (up to 600 °C/min or more) and a short holding time, usually a few minutes. The SPS process obtains fully dense samples at relatively low sintering temperatures, usually several hundred degrees lower than in the case of normal hot pressing [19]. However, there are difficulties with this method. Several authors have reported about the problem of MgB₂ decomposition during the densification at high temperatures while sintering via ex situ methods [20–22]. The MgB₂ bulk samples produced via the SPS method contain nano-sized Mg–B–O and higher borides (of compositions near MgB₄, MgB₇, MgB₁₂, MgB₁₇, and MgB₂₀), as inclusions that can be pinning centers. The quantity of secondary phase inclusions is intensified at temperatures above 900 °C, especially when ground powder (ex situ) is used. Guo et al. [23] conducted thermo-analytical studies, in which they found the onset of oxidation at 600 °C and decomposition to higher borides at 930 °C. An additional positive aspect of the SPS is its flexibility in controlling current and temperature, which is an advantage in the successive heating and cooling rates. In the first place, it was expected that this would provide good control of grain growth and, to some extent, evaporation of Mg. For MgB₂, a higher density of grain boundaries associated with a nano-structured material is desired for improved interfacial defect density and, hence, the superior flux pinning [24].

The research conducted so far has focused on the effect of the addition of nanoscopic diamond particles [25], silver [26], and rare earth particles [27] for improving the J_c of polycrystalline MgB₂. The optimal amount of nano-scale addition of diamond and Ag to MgB₂ enables the formation of high-density nano-inclusions in the MgB₂ matrix and dramatically improves J_c . In the current manuscript, we investigated the properties of high-density MgB₂ superconductors prepared using the in situ and ex situ SPS techniques. The phase and microstructure of the samples were determined by X-ray diffraction (XRD) and field-emission scanning electron microscopy (FE-SEM). Recent reports have shown the

role of sintering kinetics and precursor powders on improving flux pinning and $J_{c,S}$ [28]. Besides the advantage of the T_c , (which is around 39 K, as discussed earlier), the most important property to improve is the J_c and the upper critical fields H_{c2} . In order to achieve this, it is important to improve the pinning force and the connectivity between particles by improving the density of the MgB_2 bulk material. The explanation for our results also resides in the reduction of the cost of the application and processing time, we tried to synthesize the bulk MgB_2 samples via both the ex situ and in situ SPS methods, by using MgB_2 powder and mixing the stoichiometry ratios of Mg and B, respectively. This also aimed at fabrication of the bulk with abundant amounts of the grain-connectivity, along with high mass density, due to the respective reactions that could support even larger $J_{c,S}$ in the MgB_2 bulk samples, in both cases. The purpose of our study is to clarify the necessary conditions for high J_c using the SPS process. Here, we investigated the effects of the fabrication conditions on the crystal phase, microstructure, J_c , and flux pinning of the high density bulk in both the SPS in situ and ex situ processes, clarified the differences in the SPS processes, and investigated the method for optimizing each fabrication condition to achieve high J_c .

In this manuscript, we have focused on the production of MgB_2 by spark plasma synthesis (SPS) and physico-chemical, magnetic, and superconducting properties analysis. We emphasize that the SPS is a promising way to produce dense samples with improved grain bonding and better MgB_2 superconductor bulk densities, which could be an important variant in magnetic applications; therefore, we have dealt with this method in our work. The optimization of several parameters, such as dwell time, applied pressure, controlled heat, and current application rates, can effectively improve the immobilization of the stream and, hence, the efficiency of J_c , as discussed in this manuscript. A comparative study would enable us understand more about the effectiveness of our approach on both the ex situ and in situ processing techniques.

2. Experimental Section

Three sets of samples were synthesized and considered for this study. **The first** series of samples were fabricated by SPS with a commercially available (MgB_2 , purity >97%, 100 meshes) powder obtained commercially from Kojundo Chemicals (Laboratory Co., Ltd., Saitama, Japan). In the ex situ process, the admixed MgB_2 powder was inserted into the graphite die under ambient atmosphere and then charged into the SPS sample chamber similar to in situ synthesis. The graphite die was heated within the ranges of 800–1000 °C with the same rate of 50 °C min⁻¹ by simultaneous application of current pulses for 15 min of dwell time. Further, the dwell time was optimized by varying for 1–10 min for the sample fabricated at optimal sintering temperature of 850 °C. At the end of each process, all samples were then furnace-cooled to room temperature (RT). Final SPS ex situ products were referred as ex situ-*W-Z* where *W* and *Z* represent the sintering temperatures and the dwell times, respectively). In the overall process, after removing the bulk sample from the SPS chamber, the graphite layer and the carbon-contaminated surfaces were removed, via polishing by SiC papers. The relative bulk densities of all the samples were estimated using the theoretical density of MgB_2 . **The second** series of samples investigated in this work were prepared by the in situ SPS technique. For the in situ SPS process, 0.6 g of the Mg (99.9%, 325 mesh) and B (98.5%, 250 nm) powder obtained from Kojundo Chemicals were mixed in the ratio of 1:2 and were loaded into a \varnothing 10 mm graphite die in a glovebox filled with high pure Ar. The schematic of the SPS sample chamber is shown in Figure 1. The graphite die has an inner diameter of 10 mm. It was lined with boron nitride (BN) and was placed in the SPS apparatus (SS Alloy Co., Ltd., Higashi Hiroshima, Japan). The schematic diagram in Figure 1 also shows the cross section of the graphite die and its components. The sample chamber was evacuated and, then, filled with argon gas to a pressure of 0.5 atm. A pressure of 50 MPa was applied to the filled powder through the graphite die. The heating on the graphite commenced with the sintering temperatures being recorded for 720–775 °C ranges at the rate of 50 °C min⁻¹, and these sets of samples were named as

in situ-X-Y where X and Y are the sintering temperatures and dwell times, respectively. The third series of samples considered in this work was adopted from our previous work for the purpose of comparison with the SPS technique. The details for the experimental procedure for the in situ solid-state reaction and results are available in [27,28].

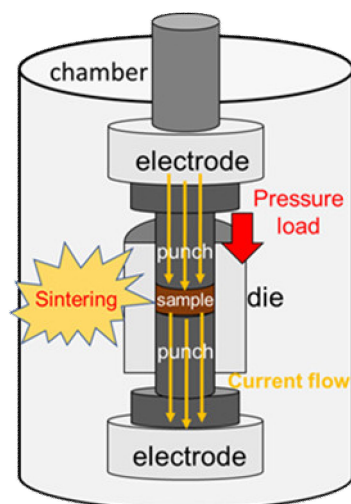


Figure 1. Schematic diagram of an SPS furnace.

To identify any impurity phases formed during sintering process, the crystal structures and constituent phases of the fabricated MgB_2 samples were investigated using a high-resolution X-ray powder diffractometer (SmartLab, Rigaku, Tokyo, Japan) using $\text{Cu-K}\alpha$ radiation ($\lambda = 1.5418 \text{ \AA}$). The XRD patterns were collected with a step size of 0.02° over a 2θ range from 20° to 80° . Small sections were cut from the bulk pellets using a diamond slow saw and polished using grinding paper sizes, ranging from 400 to 1200 grit. The sample breakthroughs were also investigated using a FE-SEM (Jeol JSM-7100F model, Nippon Electronics, Tokyo, Japan). Further microstructural and elemental characterizations were carried out by transmission electron microscope (TEM Titan Themis G2 80-200 kV X-FEG, Thermo Fisher Scientific, Waltham, MA, USA). Field and temperature dependent characterizations were carried out. Magnetization hysteresis (M - H) loops were measured in field range from 0 to 5 T at 20 K, and temperature dependence magnetization curves were recorded using a superconducting quantum interference device (SQUID) magnetometer (MPMS V model, Quantum Design, San Diego, CA, USA). Temperature dependence measurements were carried out in the zero field cooled (ZFC) regime, whereby the system is cooled with no applied field to lowest temperature. The temperature was then swept from 10 K to 50 K after applying a magnetic field of 1 mT. Sub-specimens of typical dimensions of $\sim 2.0 \times 2.0 \times 1.0 \text{ mm}^3$ were collected from each sample and were utilized for M - H and M - T measurements. The J_c values were estimated from the M - H loop based on the extended Bean critical state model using the relation:

$$J_c(H) = \frac{20 \times \Delta M(H)}{a^2 \times d(b - \frac{a}{3})} \quad (1)$$

The parameters in the relation can be summarized where d denotes the sample thickness, a and b are the cross sectional dimensions with $b \geq a$, and ΔM is the difference of the magnetic moments during increasing and decreasing field in M - H loop [29].

3. Results and Discussion

3.1. Ex Situ Synthesis

The XRD patterns for the MgB_2 bulks produced by ex situ sintering at various sintering temperatures from 800–1000 °C for 15 min are shown in Figure 2. The XRD also show a

small amount of MgO in the starting powder, which was included for comparison. The X-ray diffraction patterns of all the samples show that the highest intensity Bragg peaks are representing the MgB₂ phase as major. However, as the sintering temperature increased, the decomposition increased mainly to MgB₄ and MgO as impurity phases. The presence of MgO and MgB₄ impurity phases is not uncommon in MgB₂ processing, and the relatively high contents of the observed impurity phases in these samples are related to the high processing temperatures used [23,24]. A sequel to the updated phase diagram of Mg–B system at high temperature, the Mg vapor is present in equilibrium with MgB₂ or MgB₄ [30]. The observed increase in the contents of MgB₄ and MgO is expected if MgO forms from reaction of the Mg vapor [20]. However, there is the tendency of resolving this issue by improving the quality of the starting powder; hence, by carrying out powder processing in an inert dry atmosphere or by possible reduction in the processing temperature [20,21]. The decomposition was observed to intensify when the sintering temperature was increased above 850 °C. However, compared to the reported literature [31], the effect of the low proportions of the formed secondary phase was seen in the improvement of the flux pinning characteristics due to the refinement of the grains, which was articulated later in the sample microstructure.

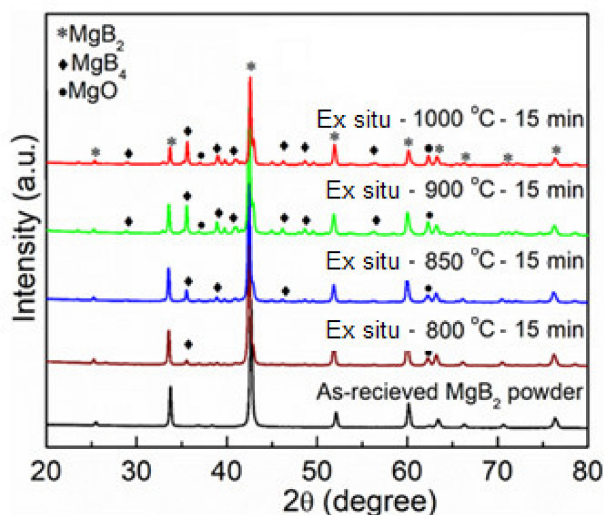


Figure 2. X-ray diffraction patterns for sintering temperature optimization of spark plasma sintered MgB₂ bulk via the ex situ method.

The polycrystalline MgB₂ sample density was determined to be 1.73 g/cm³, and the corresponding relative densification value is 66%. The density of the ex situ - 800 °C - 15 min to ex situ - 1000 °C - 15 min samples was found to be 2.41 g/cm³–2.59 g/cm³, which corresponds to 92–99% of the theoretical density of the same compound. The densification values are given in Table 1. It was observed that as the sintering temperature increased, the relative density values were increased gradually, which indicates the decrease of grain boundary in the bulk samples. The density of the SPS bulk samples is improved about 30%, which implies that grain connectivity is improved tremendously in the case of SPS MgB₂ bulk samples. The achieved density in the MgB₂ bulk samples is comparable with those reported by the literature on the same compound fabricated by SPS and even hot-press [32]. With the present results, we successfully fabricated highly dense MgB₂ bulk samples using the SPS technique.

Table 1. The polycrystalline MgB₂ sample density was determined to be 1.73 g/cm³, and the corresponding relative densification value is 66%. The density of the ex situ - 800 °C - 15 min–ex situ-1000 °C - 15 min samples was found to be 2.41–2.59 g/cm³, which corresponds to 92–99% of the theoretical density of the same compound. The densification values for dwell time, relative density, and superconducting transition ($T_{c(\text{onset})}$, $T_{c(\text{offset})}$, ΔT_c) for samples prepared by the ex situ and in situ methods. The standard deviation(s) for $T_{c,S}$ and $\Delta T_{c,S}$: $\sigma < 0.21$.

Sample	Dwell Time (min)	Relative Density (%)	Superconducting Transition (K)			Phase
			$T_{c(\text{onset})}$	$T_{c(\text{offset})}$	ΔT_c	
Ex Situ						
Ex situ_1000 °C	15	99	38.3	37.7	0.6	Decomposition present
Ex situ_900 °C	15	99	38.2	37.7	0.5	Decomposition present
Ex situ_850 °C	15	97	38.2	37.7	0.4	Decomposition reduced
Ex situ_800 °C	15	92	38.1	37.7	0.4	Little decomposition
Ex situ_850 °C	10	97	38.3	38.0	0.3	Improved phase/little MgO
Ex situ_850 °C	5	89	38.1	37.8	0.3	Improved phase/little MgO
Ex situ_850 °C	1	86	38.5	37.9	0.6	Little MgO
In Situ						
In situ_775 °C	Tubular/3 h	66	38.5	38.1	0.3	Little MgO
In situ_775 °C	SPS/20	90	38.3	38.0	0.3	MgO/MgB ₄
In situ_775 °C	SPS/15	90	38.4	38.2	0.2	Little MgO
In situ_750 °C	SPS/15	88	38.3	38.1	0.3	Little MgO
In situ_720 °C	SPS/15	83	38.5	38.3	0.2	Little MgO

To further control the decomposition that occurred at 850 °C in the SPS MgB₂ bulk sample, the dwell time was varied and the observed XRD patterns are shown in Figure 3. It was observed that as the dwell time decreased from 15 min to 1 min, the decomposition was effectively decreased. The densification values are shown in Table 1. These are the calculated values of the relative bulk densities. As the dwell time is controlled for each stage of synthesis from 15 min to 1 min, the densification was decreased from 97% to 86%, indicating that the dwell time is also an important parameter. With the resent results, it can be observed that the sintering temperature of 850 °C and a 10 min dwell is the best condition, which shows minimal decomposition with relatively high densification values.

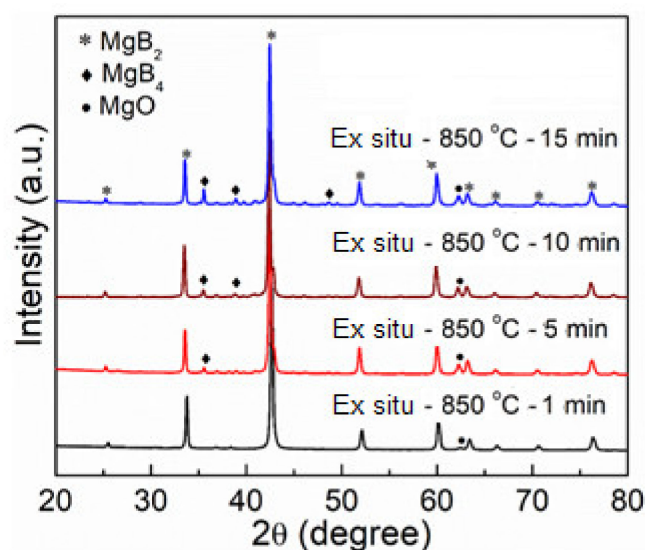


Figure 3. The X-ray diffraction patterns for MgB₂ ex situ further optimization at 850 °C.

The DC magnetic susceptibility curves that are normalized by the maximum superconducting values for ex situ - 800 °C - 15 min measured to ex situ - 1000 °C - 15 min samples are shown in Figure 4a, and the dwell time-varied ex situ-850 °C - 1 min to ex situ - 850 °C - 15 min samples are shown on the Figure 4b. A polycrystalline MgB₂ sample supercon-

ducting transition curve is also included as reference. The onset of T_c for Polycrystalline MgB_2 is determined to be 38.5 K with transition width (ΔT_c) of 0.43 K. All samples show sharp superconducting transitions at the onset value of >38 K with ΔT_c of <1 K), indicating the high quality nature of the fabricated MgB_2 bulks. Presently, our T_c results showed a negligible reduction in the onset value of bulk samples compared to the polycrystalline sample. The width of the superconducting transitions ΔT_c of all the samples was observed to slightly decrease in both the ex situ and in situ processes, as the processing temperature decreases at a controlled dwell time. The gradual degradation of the T_c could have resulted from the impurity phases. This was supported by Yakinci et al. [33].

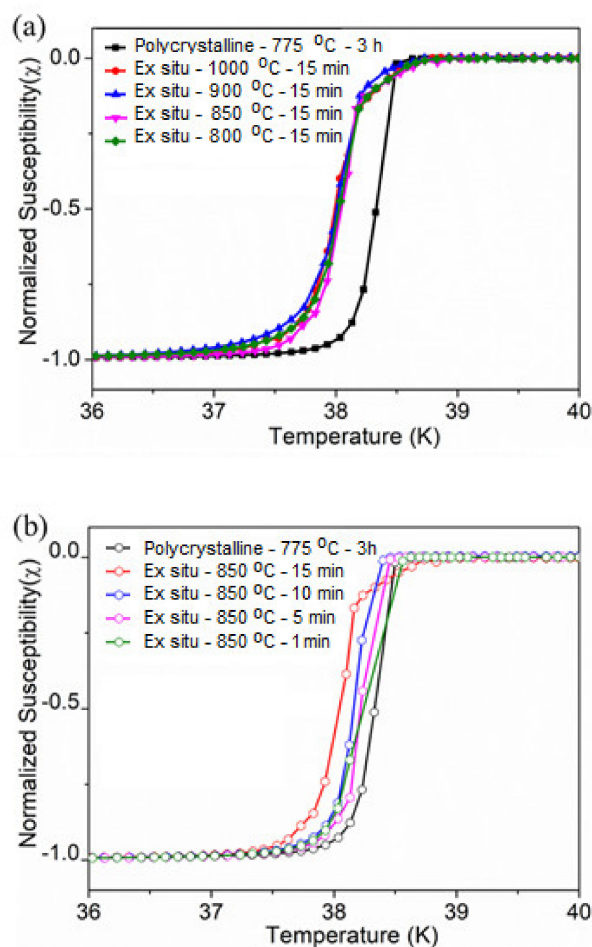


Figure 4. Superconducting transition in the bulk MgB_2 processed by SPS via ex situ (a) variation of the sintering temperature and (b) variation of the dwell time.

The field dependence of $J_c(B)$ of the MgB_2 samples at 20 K was estimated utilizing the extended Bean critical state model [29]. Figure 5a shows the variation of J_c curves of MgB_2 bulk ex situ samples synthesized at different sintered temperatures of 800 °C, 850 °C, 900 °C, and 1000 °C. Self-field J_c [$J_c(0)$] values for the samples are determined to be 401, 493, 413, and 333 kA/cm², respectively. The $J_c(0)$ value for the Polycrystalline MgB_2 sample is 298 kA/cm², which clearly shows that the MgB_2 bulk samples support carrying large J_c compared to the sample produced by the conventional sintering method. Among, the SPS-processed MgB_2 samples, ex situ - 850 °C - 15 min superconductor was observed to be superior in the J_c performance, which could be attributable to the high density along with the relatively lower fraction of the secondary phase formation, as indicated on the sample XRD. Moreover, even though the densification values are higher in the case of the 900 °C and 1000 °C sintered samples, J_c performance is inferior and worsened as the sintering temperature increased. This is mainly due to the MgB_2 phase degradation into fractions of

non-superconducting phases. To further control this effect, we tried to control the regime of the sintering process. The $J_c(H)$ curves determined at 20 K for the ex situ - 850 °C - 1 min to ex situ - 850 °C - 15 min superconductors are shown in Figure 5b. The self-field J_c of the ex situ - 850 °C - 1 min, ex situ - 850 °C - 5 min, ex situ - 850 °C - 10 min, and ex situ - 850 °C - 15 min superconductors are determined to be 420 kA/cm², 495 kA/cm², 517 kA/cm², and 493 kA/cm², respectively. The MgB₂ ex situ bulk synthesized at 850 °C for 10 min exhibited superior field dependence J_c performance. Presently, our results are superior to the reports available in the literature on the MgB₂ bulks produced by SPS and HP [28,32]. The superior field dependence properties of the ex situ - 850 °C - 15 min superconductor could be attributable to the optimal sintering temperature and controlled dwell time, at which the phase degradation was minimal with a corresponding improvement in the density. With this, we successfully fabricated highly dense MgB₂ bulk samples via the ex situ SPS method, and, mainly, such high densification values are achieved at lower sintering temperatures.

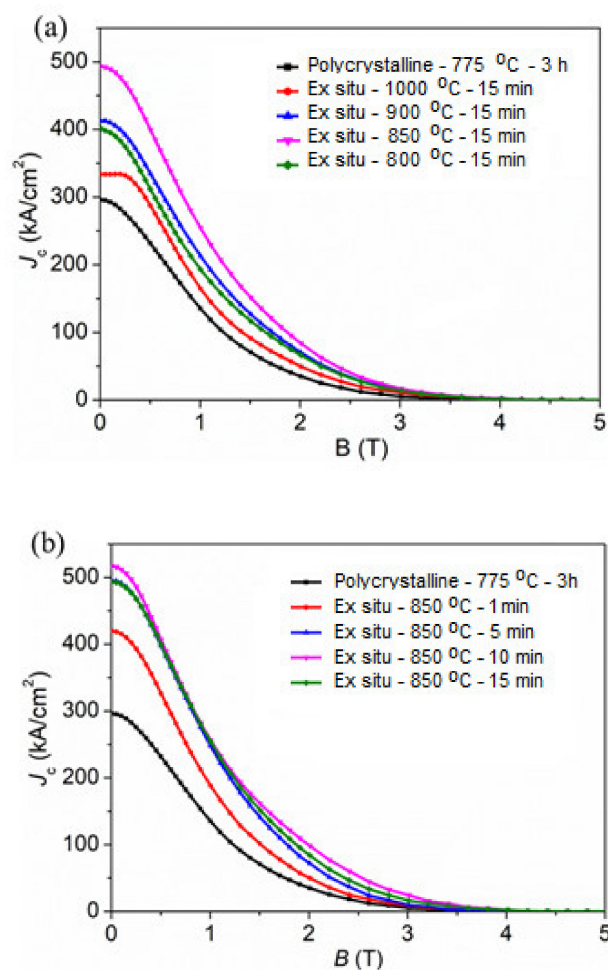


Figure 5. The magnetic field dependence of J_c curves determined at 20 K for MgB₂ bulk superconductors fabricated by the SPS ex situ method for (a) sintering temperature variation and (b) dwell time variation.

3.2. In Situ Synthesis

In the above sections, we produced MgB₂ bulk superconductors with high mass density supporting large critical currents via the ex situ SPS method. However, in order to reduce the cost of the application and the time, we attempted to synthesize the MgB₂ bulk samples via the in situ SPS method by mixing the stoichiometry ratios of Mg and B. This also aimed at fabrication of the bulk with abundant amounts of grain connectivity along

with high mass density due to the in situ reaction, which could support even larger $J_{c,S}$ in the MgB_2 bulk samples. The in situ process for the phase analysis is shown in Figure 6, and the observed XRD was compared to our previously fabricated bulk sample using the in situ solid state sintering technique by the tubular furnace at 775 °C for 3 h.

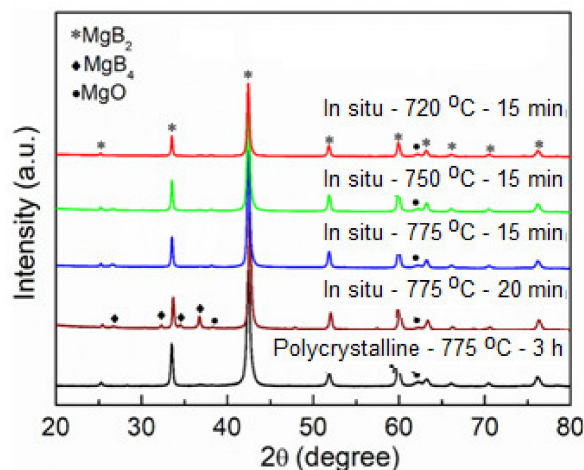


Figure 6. X-ray diffraction patterns for spark plasma sintered MgB_2 bulk via the in situ method.

At first, we tried to synthesize the in situ MgB_2 bulk by SPS using the same temperature condition but with a longer dwell time of 20 min. With the occurrence of decomposition at this condition, we proceeded by slightly decreasing the dwell time and controlling the sintering temperatures, which was found to be effective for decreasing the deterioration of the MgB_2 phase; however, it was necessary to find the optimum temperature for high-density conditions, at which we could also attain an equilibrium for the superconducting performance of our bulk in situ samples. The superconducting transitions in the MgB_2 bulk synthesized by the in situ process are shown in Figure 7. The Figure 8 shows the superconducting field performances of the J_c of the in situ process.

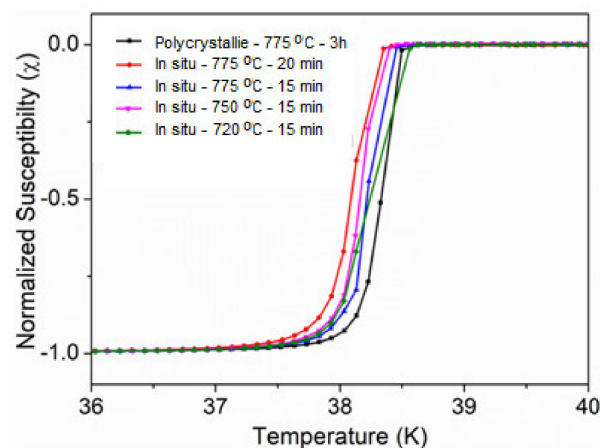


Figure 7. The superconducting transitions in the MgB_2 bulk synthesized by in situ process.

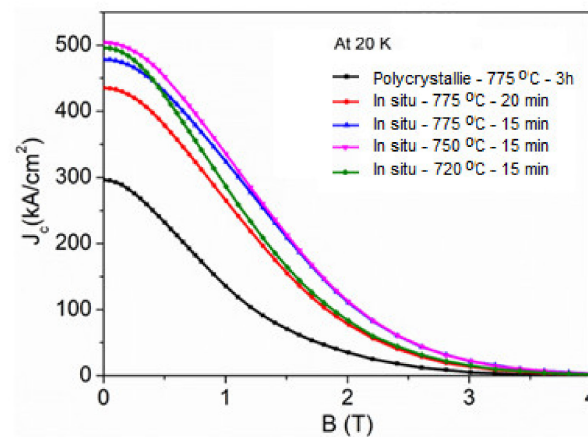


Figure 8. Shows the superconducting field performances of the J_c of the in situ process.

Besides the contributions of secondary particles, one of the important observations we made was the significant increase in the SPS in situ sample density, by sole temperature control and grain size refinement; while keeping the initial pressure of 50 MPa, we could achieve ~90% density. This could be a breakthrough when further optimization by pressure increase is employed, since this could exceed the findings of Prikhna et al. [31] for the highest density obtained by the SPS in situ process and, hence, the superconducting performance and mechanical properties.

More crystallinity was observed for the in situ samples than the ex situ samples, which is evident in the degree of sharpness for the superconducting transitions. The observed suppression in the ex situ samples T_c could be due to the effect of the impurity phases, which occurred in the XRD analysis. This observation on the slight suppression in the T_c was supported by Dancer et al. [34]. This suggests that the lower processing temperatures could have attained a degree of sufficiency in recovering the disorder that may have existed in the initial (as received) powders.

All the samples tend to show improvement in the field performance, when compared to the bulk synthesized via tubular furnace; however, the in situ processed bulk sample at 750 °C was optimal at 504 kA/cm² at 88% packing density for these sets of samples. This is so promising, when compared to the recent reports of Noudem et al. [28] for in situ processing at 500 kA/cm² and 84% packing density. We suggest that the field dependence of the respective J_c varies with temperature optimization as a function of the grain size refinement and, hence, the densities. The additional pinning centers in this case may also have resulted from the nano-sized particles, which also maximize the flux pinning performance exhibited by our best sample bulks; meanwhile, we also proposed that the relevance of the J_c improvement is also attributed to the contribution of the refinement of the grains, which improved the flux pinning performance and consequently the J_c .

3.3. Microstructural Analysis

The grain size and grain connectivity are crucial for determination of the J_c in polycrystalline superconductors. Microstructural characterization carried out via FESEM on the ex situ - 850 °C - 10 min and in situ - 750 °C - 15 min samples are compared with Polycrystalline MgB₂ sample in Figure 9a–c, respectively. The statistical analysis of the grain size is completed using the ImageJ program, and the corresponding size histograms are shown in Figure 9d–f, respectively. The mean size of the MgB₂ grains for polycrystalline MgB₂, ex situ - 850 °C - 10 min, and in situ - 750 °C - 15 min samples, are determined to be 112 nm, 119 nm, and 132 nm, respectively. These results vindicate that the MgB₂ bulk samples produced via SPS contain slightly finer sized MgB₂ superconducting grains than the polycrystalline MgB₂ sample. It is interesting to note here, even though both the ex situ - 850 °C - 10 min and in situ - 750 °C - 15 min samples are fabricated by the SPS method, the frequency of fine-sized grains is larger in the case of the former sample. This could

be as a result of the further and careful optimization of the dwell time during the ex situ processing, which could have further controlled the grain sizes.

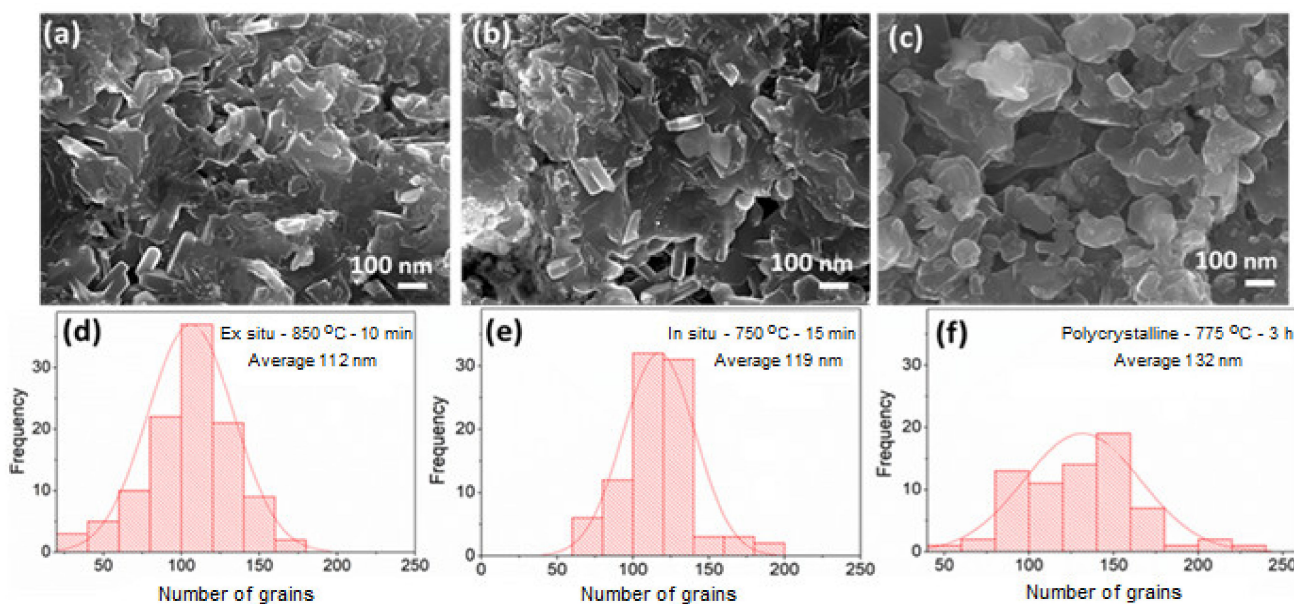


Figure 9. High magnification (30,000 \times) FE-SEM images for optimized fractured bulk samples produced by (a) SPS ex situ, (b) SPS in situ, and (c) polycrystalline MgB_2 . The subfigures (d–f) shows the statistical analysis of the grain size distributions.

In order to complement our FESEM observations, we further conducted microstructural analyses via TEM investigations, as shown in Figure 9, on ex situ - 850 $^{\circ}\text{C}$ - 10 min and in situ - 750 $^{\circ}\text{C}$ - 15 min samples. We could suggest the occurrence of the nano-size MgO particles, which may have enhanced the flux pinning of the SPS processed samples, implying that the interactive contributions of the refined grains and the MgO inclusions could have been the primary source of the improved superconducting performance. In ex situ SPS processing, our observation for the optimized sample indicated the presence of nano-size grains of MgB_4 , as shown in Figure 10a, which could have been a contributor to supporting the superconducting J_c . The TEM results for these samples in Figure 10a showed more refined grains of MgB_4 as a secondary phase and, also, what could possibly be the inclusion of the MgO particles. We suppose that the dramatic increase in the superconducting J_c is attributed to this effect. As for the in situ process, the microstructure reveals the occurrence of the MgO system within the MgB_2 matrix for the optimized conditions, but more grains tend to manifest with a shorter dwell time, resulting in better connectivity and more controlled inclusion of the MgO , as illustrated in Figure 10b.

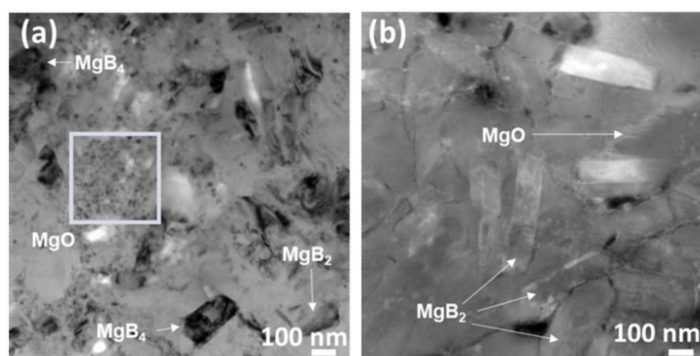


Figure 10. TEM micrographs of optimized polished surfaces of (a) SPS ex situ and (b) SPS in situ.

Our findings indicate that both the SPS-processed bulk samples are superior compared to the polycrystalline sample. It could be emphasized here that the grain refinement, by virtue of the grain sizes, connectivity, and the resulted improved densities, aided in enhancing the J_c . Among bulk samples, they exhibit different flux pinning behaviors as the slopes of the J_c curves are different at different fields. This clearly indicates that the clean grain boundary and lower porosity, along with the relatively higher densification, are supporting high $J_{c,S}$ at moderate-applied magnetic fields, along with the nano-sized secondary phases, as observed from TEM. With this, we successfully synthesized the MgB₂ bulk samples via the in situ method by SPS in its pure phase. Present self-field results are slightly inferior compared to ex situ bulks. However, it should be noted here that the in situ bulks are of low densification compared to ex situ, but still exhibit higher quality the bulk samples compared to a recent report [28]. By further optimization of the processing parameters, high-quality MgB₂ bulks can be fabricated, which support even superior field dependence properties compared to any other method. In our case, the processing temperature and dwell time were the variable parameters considered to be effective.

3.4. Flux Pinning Analysis

To support our discussions regarding the TEM analysis, the pinning force, f_p , was investigated using a scaling method based on the body of literature data and then compared to our studies. We calculated the scaling behavior and the best fits to the theory using the scaling methods of Dew-Hughes [35] and Kramer [36]. Flux pinning of the fabricated MgB₂ bulk samples is scaled using the Dew-Hughes general expression.

$$f_p = A \cdot (h)^p \cdot (1 - h)^q \quad (2)$$

Constants p and q are describing the actual pinning mechanism. The normalized flux pinning force density is denoted by $f_p = F_p/F_{p,max}$, and the reduced magnetic field is $h = H/H_{irr}$. The value of the irreversibility field, H_{irr} , was estimated as the field where J_c decreased to 100 A/cm² at 20 K, which is customary in our works. The normalized pinning force $F_p/F_{p,max}$ versus the reduced fields were plotted, and the curves are shown in Figure 11. According to Dew-Hughes, the peak position of the $f_p(h)$ dependence indicates the type of pinning in the superconducting material. As per the model, the peak position of f_p vs. h at 0.2 implies grain boundary pinning, meanwhile 0.33 implies core, δT_c pinning, and so on. This flux pinning behavior was also supported by the works of Koblishka et al. [37] on the pinning force scaling analysis for high- T_c superconductors. The resulting peak positions, h_o , were found around ~0.25 and ~0.28, respectively, for the optimized in situ and ex situ samples, with a slight shift to the right towards higher field that supports the indication for particle pinning. The implication here is that some of contributions by the flux pinning may have resulted from nano-sized inclusions of the secondary phases; this assertion is also supported in the TEM analysis discussed in Figure 10. However, the polycrystalline bulk sample tends to exhibit the ideal peak position, which is around 0.22, indicating the effect of grain boundaries for vortex pinning. The shifts in the peak positions could also be attributed to the improved connectivity and the resulting refined grains, which added to our high suspicion of the temperature control and dwell time during synthesis. The mechanism for pinning other than grain boundaries for MgB₂, was emphasized by other reports [38], which also supports our findings. The Figure 11 shows the flux pinning diagram showing peak positions for the optimized in situ and ex situ samples compared with polycrystalline MgB₂.

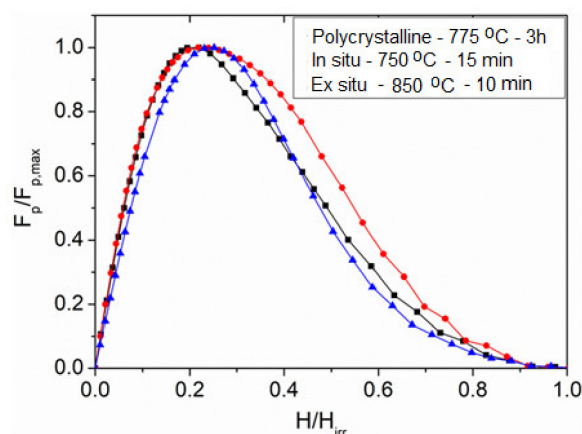


Figure 11. The flux pinning diagram showing peak positions for the optimized in situ and ex situ samples compared with polycrystalline MgB₂. There is a slight shift in peak positions to the right.

4. Conclusions

We discussed the influence of the sintering temperature and dwell time on J_c - B properties of dense in situ and ex situ MgB₂ bulks synthesized by SPS. However, it is obvious that the J_c - B characteristics improved as a result of appropriate nano-inclusions of MgO and MgB₄ impurity phases in the final microstructure, which resulted in significant flux pinning enhancement. For in situ and ex situ, the best samples demonstrated self-field J_c behaviors at 504 and 517 kA/cm², respectively. The good grain refinement and connection, which also influenced the high bulk densities, may have resulted in more improved J_c behaviors. Nevertheless, the ex situ synthesis is complicated and time-consuming, despite the challenges in controlling the impurity phases. We proposed that it might be appropriate to consider the in situ processing method of synthesizing high density MgB₂ bulk, which is less complicated and saves time with its ease of control for the impurity phase. Meanwhile, more progress can be achieved for the SPS in situ processing by improving the quality of starting powders and applying high-pressure sintering. Our approach also supports the possibilities of other processing windows in which well-sintered MgB₂ cores in wires and bulk magnets can be fabricated for practical applications.

Author Contributions: Conceptualization, J.L.D., N.S., T.O. and M.M.; methodology, J.L.D., S.P.K.N., J.S. and H.O.; formal analysis, J.L.D., S.P.K.N., P.P., J.S. and N.S.; investigation, J.L.D., J.S., N.S., T.W. and A.W.; resources and literature review, J.L.D., S.P.K.N., P.P., H.O. and N.S.; writing—original draft preparation, J.L.D. and N.S.; writing—review and editing, Y.K. All authors; visualization, J.L.D., S.P.K.N., P.P. and N.S.; supervision and validation, N.S. and M.M.; project administration, J.L.D., N.S. and M.M. All authors have read and agreed to the published version of the manuscript.

Funding: This research received no external funding.

Institutional Review Board Statement: Not applicable.

Informed Consent Statement: Not applicable.

Data Availability Statement: The data presented in this study are available on request from the corresponding author.

Conflicts of Interest: The authors declare no conflict of interest. The funders had no role in the research design, data collection, analyses, interpretation, writing the manuscript, or publishing the results.

References

1. Russell, V.; Hirst, R.; Kanda, F.A.; King, A.J. An X-ray study of the magnesium borides. *Acta Cryst.* **1953**, *6*, 870. [[CrossRef](#)]
2. Nagamatsu, J.; Nakagawa, N.; Muranaka, T.; Zenitani, Y.; Akimitsu, J. Superconductivity at 39 K in magnesium diboride. *Nature* **2001**, *410*, 63. [[CrossRef](#)] [[PubMed](#)]

3. Murakami, A.; Noudem, J.; Guesmi, Z.; Kudo, T.; Iwamoto, A. Mechanical properties of MgB₂ bulk fabricated by spark plasma sintering. *Phys. Procedia* **2015**, *65*, 77–80. [[CrossRef](#)]
4. Murakami, A.; Iwamoto, A.; Noudem, J.G. Mechanical properties of bulk MgB₂ superconductors processed by spark plasma sintering at various temperatures. *IEEE Trans. Appl. Supercond.* **2018**, *28*, 8400204. [[CrossRef](#)]
5. Eisterer, M.; Zehetmayer, M.; Weber, H.W. Current Percolation and Anisotropy in polycrystalline MgB₂. *Phys. Rev. Lett.* **2003**, *90*, 247002. [[CrossRef](#)]
6. Miryala, M.; Arvapalli, S.S.; Sakai, N.; Murakami, M.; Mochizuki, H.; Naito, T.; Fujshiro, H.; Jirsa, M.; Murakami, A.; Noudem, J. Complex pulse magnetization process and mechanical properties of spark plasma sintered bulk MgB₂. *Mat. Sci. Eng. B* **2021**, *273*, 115390. [[CrossRef](#)]
7. Noudem, J.G.; Dupont, L.; Gozzelino, L.; Bernstein, P. Superconducting properties of MgB₂ bulk shaped by spark plasma sintering. *Mater. Today Proc.* **2016**, *3*, 545. [[CrossRef](#)]
8. Gajda, D.; Morawski, A.; Zaleski, A.J.; Kurnatowska, M.; Cetner, T.; Gajda, G.; Presz, A.; Rindfleisch, M.; Tomsic, M. The influence of HIP on the homogeneity, J_c , J_{c0} , T_c and F_p in MgB₂ wires. *Supercond. Sci. Technol.* **2014**, *28*, 015002. [[CrossRef](#)]
9. Gajda, D.; Morawski, A.; Zaleski, A.J.; Häßler, W.; Nenkov, K.; Rindfleisch, M.A.; Żuchowska, E.; Gajda, G.; Czujko, T.; Cetner, T.; et al. The critical parameters in *in-situ* MgB₂ wires and tapes with ex-situ MgB₂ barrier after hot isostatic pressure, cold drawing, cold rolling and doping. *J. Appl. Phys.* **2015**, *117*, 173908. [[CrossRef](#)]
10. Shim, S.H.; Shim, K.B.; Yoon, J.W. Superconducting characteristics of polycrystalline MgB₂ ceramics fabricated by a spark plasma sintering technique. *J. Am. Ceram. Soc.* **2015**, *88*, 858. [[CrossRef](#)]
11. Aldica, G.; Batalu, D.; Popa, S.; Ivan, I.; Nita, P.; Sakka, Y.; Vasyukiv, O.; Miu, L.; Pasuk, I.; Badica, P. Spark plasma sintering of MgB₂ in the two-temperature route. *Phys. C Supercond.* **2012**, *477*, 43. [[CrossRef](#)]
12. Larbalestier, D.; Gurevich, A.; Feldmann, D.M.; Polyanskii, A. High- T_c superconducting materials for electric power applications. *Nature* **2001**, *410*, 368. [[CrossRef](#)]
13. Braccini, V.; Nardelli, D.; Penco, R.; Grasso, G. Development of ex-situ processed MgB₂ wires and their applications to magnets. *Phys. C Supercond.* **2007**, *456*, 209. [[CrossRef](#)]
14. Glowacki, B.A.; Majoros, M.; Vickers, M.; Evetts, J.E.; Shi, Y.; McDougall, I. Superconductivity of powder-in-tube MgB₂ wires. *Supercond. Sci. Technol.* **2001**, *14*, 193. [[CrossRef](#)]
15. Yi, J.H.; Kim, K.T.; Jun, B.-H.; Joo, J.; Shon, J.M. Pore formation in *in-situ* processed MgB₂ superconductors. *Phys. C Supercond.* **2009**, *469*, 1192. [[CrossRef](#)]
16. Jo, W.; Huh, J.-U.; Ohnishi, T.; Marshall, A.F.; Beasley, M.R.; Hammond, R.H. *In-situ* growth of superconducting MgB₂ thin films with preferential orientation by molecular-beam epitaxy. *Appl. Phys. Lett.* **2002**, *80*, 3563. [[CrossRef](#)]
17. Zeng, X.H.; Sukiasyan, A.; Xi, X.X.; Hu, Y.F.; Wertz, E.; Li, Q. Superconducting properties of nanocrystalline MgB₂ thin films made by an in situ annealing process. *Appl. Phys. Lett.* **2001**, *79*, 1840. [[CrossRef](#)]
18. Liu, Y.; Cheng, F.; Qiu, W.; Ma, Z.; Hossain, S.; Dou, S.X. High performance MgB₂ superconducting wires fabricated by improved internal Mg diffusion process at a low temperature. *J. Mat. Chem. C* **2016**, *4*, 9469–9475. [[CrossRef](#)]
19. Giunchi, G.; Ceresara, S.; Ripamonti, G.; Di Zenobi, A.; Rossi, S.; Chiarelli, S.; Spadoni, M.; Wesche, R.; Bruzzone, P.L. High performance new MgB₂ superconducting hollow wires. *Supercond. Sci. Technol.* **2003**, *16*, 285. [[CrossRef](#)]
20. Fan, Z.Y.; Hinks, D.; Newman, N.; Rowell, J. Experimental study of MgB₂ decomposition. *Appl. Phys. Lett.* **2001**, *79*, 87. [[CrossRef](#)]
21. Schmitt, R.; Glaser, J.; Wenzel, T.; Nickel, K.; Meyer, H.-J. A reactivity study in the Mg-B system reaching for an improved synthesis of pure MgB₂. *Phys. C Supercond.* **2006**, *436*, 38. [[CrossRef](#)]
22. Brutti, S.; Balducci, G.; Gigli, G.; Ciccio, A.; Manfrinetti, P.; Palenzona, A. Thermodynamic and kinetic aspects of decomposition of MgB₂ in vacuum: Implications for optimization of synthesis conditions. *J. Cryst. Growth* **2006**, *289*, 578. [[CrossRef](#)]
23. Guo, Y.; Zhang, W.; Yang, D.; Yao, R.-L. Decomposition and oxidation of magnesium diboride. *J. Am. Ceram. Soc.* **2012**, *95*, 754. [[CrossRef](#)]
24. Kang, D.-K.; Kim, D.-W.; Kim, C.-J.; Ahn, I.-S. The Phase Analysis of Spark Plasma Sintered MgB₂ After Ball Milling. *J. Nanosci. Nanotechnol.* **2010**, *10*, 142. [[CrossRef](#)] [[PubMed](#)]
25. Dadiel, L.J.; Muralidhar, M.; Murakami, M. Flux pinning and superconducting properties of MgB₂-diamond nanocomposites. *J. Phys. Conf. Ser.* **2017**, *1054*, 313.
26. Dadiel, L.J.; Muralidhar, M.; Murakami, M. Improved superconducting performance of Ag-added nano-diamond doped MgB₂. *Proc. SPIE* **2019**, *11054*, 110540I.
27. Ojha, N.; Varma, G.D.; Singh, H.K.; Awana, V.P.S. Effect of rare-earth doping on the superconducting properties of MgB₂. *J. Appl. Phys.* **2009**, *105*, 07E315. [[CrossRef](#)]
28. Noudem, J.G.; Yiteng, X.; Pierre, B.; Richard, R.; Masaki, H.; Srikanth, S.A.; Miryala, M.; Masato, M. Improvement of critical current density of MgB₂ bulk superconductor processed by Spark Plasma Sintering. *J. Amer. Ceram. Soc.* **2020**, *103*, 6169–6175. [[CrossRef](#)]
29. Chen, D.; Goldfarb, R.B. Kim model for magnetization of type-II superconductors. *J. Appl. Phys.* **1989**, *66*, 2489–2500. [[CrossRef](#)]
30. Balducci, G.; Brutti, S.; Ciccio, A.; Gigli, G.; Manfrinetti, P.; Palenzona, A.; Butman, M.F.; Kudinc, L. Thermodynamics of the intermediate phases in the Mg-B system. *J. Phys. Chem. Solids* **2005**, *66*, 292. [[CrossRef](#)]
31. Prikhna, T.; Noudem, J.; Gawalek, W.; Mamalis, A.; Soldatov, A.; Savchuk, Y.; Moshchil, V.; Eisterer, M.; Weber, H.W.; Dub, S.; et al. Spark plasma synthesis and sintering of superconducting MgB₂-based materials. *Mat. Sci. Forum* **2012**, *721*, 3. [[CrossRef](#)]

32. Häßler, W.; Scheiter, J.; Hadrich, P.; Kauffmann-Weiß, S.; Holzapfel, B.; Oomen, M.; Nielch, K. Properties of ex-situ MgB₂ samples prepared by uniaxial hot pressing and spark plasma sintering. *Phys. C Supercond. Appl.* **2018**, *551*, 48. [[CrossRef](#)]
33. Yakıncı, M.E.; Balcı, Y.; Aksan, M.A.; Adiguzel, H.I.; Gencer, A. Degradation of Superconducting Properties in MgB₂ by Formation of the MgB₄ Phase. *J. Supercond.* **2002**, *15*, 607. [[CrossRef](#)]
34. Dancer, C.E.J.; Prabhakaran, D.; Basoglu, M.; Yanmaz, E.; Yan, H.; Reece, M.; Todd, R.I.; Grovenor, C.R.M. Fabrication and properties of dense ex-situ magnesium diboride bulk material synthesized using spark plasma sintering. *Supercond. Sci. Technol.* **2009**, *22*, 095003. [[CrossRef](#)]
35. Dew-Hughes, D. Flux pinning mechanisms in type-II superconductors. *Philos. Mag.* **1974**, *30*, 293. [[CrossRef](#)]
36. Kramer, E.J. Scaling laws for flux pinning in hard superconductors. *J. Appl. Phys.* **1973**, *44*, 1360. [[CrossRef](#)]
37. Koblischka, M.; Muralidhar, M. Pinning force scaling analysis of Fe-based high-*T_c* superconductors. *Int. J. Mod. Phys. B* **2016**, *30*, 1630017. [[CrossRef](#)]
38. Kario, A.; Nast, R.; Häßler, W.; Rodig, C.; Mickel, C.; Goldacker, W.; Holzapfel, B.; Schultz, L. Critical current density enhancement in strongly reactive ex situ MgB₂ bulk and tapes prepared by high energy milling. *Supercond. Sci. Technol.* **2011**, *24*, 075011. [[CrossRef](#)]